Journal of
Instrumentation

Standardizing high electron temperature measurement comparisons: a method for cross-diagnostic and cross-machine analysis

Published by IOP Publishing for Sissa Medialab

Received: *March 26, 2025*
Accepted: *July 28, 2025*
Published: *September 17, 2025*

7th International Conference Frontiers in Diagnostic Technologies
INFN research center of Frascati, Italy
21–23 October 2024

Standardizing high electron temperature measurement comparisons: a method for cross-diagnostic and cross-machine analysis

L. Senni[a,b,*] **F.P. Orsitto**[a,c] **M. Fontana**[d] **S. Mazzi**[e] **E. Giovannozzi**[c] **and G. Giruzzi**[e]

[a] *Institute for Applied Mathematics (IAC) - CNR, Roma, Italy*
[b] *Department of Astronautical, Electrical and Energy Engineering, Sapienza University of Rome, Rome, Italy*
[c] *Department Fusion and Technology for Nuclear Safety, ENEA, C.R. Frascati, Frascati (Rome), Italy*
[d] *Tokamak Energy Ltd, Milton Park, Oxfordshire OX14 4SD, U.K.*
[e] *Institute for Magnetic Fusion Research (IRFM) - CEA, F-13108 Saint-Paul-lez-Durance, France*

E-mail: luca.senni@cnr.it

Abstract: In tokamaks, measuring electron temperatures in the plasma core may be quite challenging, especially when they exceed 6–8 keV [1]. Discrepancies are detected between the values measured by different diagnostics, such as Thomson Scattering (TS) and Electron Cyclotron Emission (ECE), which are expected to agree. Accurate and reliable determination of electron temperature in high-temperature scenarios, is crucial for the development of future reactors like ITER and Demo (with ITER's core plasma expected to have an electron temperature of about 25 keV) [2], as well as for the Chinese Fusion Engineering Test Reactor (CFETR) [3]), in which discrepancies in electron temperature measurements could be even more pronounced. Resolving this diagnostic issue is crucial because it implies a deep understanding of important aspects of plasma physics in the core and beyond. Recently, further studies on this topic have yielded substantial results and clarified several aspects [9–12]. Current research focuses on the possible causes of the local non-Maxwellian shape of the electron energy distribution function, which is at the root of these discrepancies [1, 4–12]. Ongoing research by various groups

*Corresponding author.

https://doi.org/10.1088/1748-0221/20/09/C09009

working on magnetic confinement machines worldwide aims to address this long-standing issue within the framework of an ITPA (International Tokamak Physics Activity) initiative.

This paper proposes a method to compare data collected by ECE and TS, which is based upon previously developed techniques for analyzing JET data [1], and is implemented in a dedicated Python code, to tackle issues identified in recent years, while also ensuring the output is comparable across different machines. The goal is to perform comparisons under consistent conditions, irrespective of machine-specific factors such as dimensions, fields, and coordinates. The methods developed and the corresponding implementations in a code, addresses several critical aspects, including the positions of measurements, i.e. the plasma position relative to the diagnostics' lines of sight (LoS), the involved volumes, and other controls to ensure uniformity of results during multi-shot analyses. These controls encompass acquisition rate, data interpolation, and the equilibrium reconstruction codes employed, with the objective of obtaining the best possible comparison between the two diagnostics.

KEYWORDS: Data processing methods; Nuclear instruments and methods for hot plasma diagnostics

2025 JINST 20 C09009

Contents

1 Introduction

The measurement of the electron temperature is fundamental in magnetically confined fusion plasmas, and accurate, reliable values are necessary for plasma control as well as for many other analyses. The temperature profiles also form the basis for various simulations and approximations. In particular, they are crucial in the plasma core, where high-energy electrons can introduce uncertainties in the measurements, and different values may be detected with different diagnostics, often lying well outside the possible error bars or calibration errors. These differences are caused by a non-Maxwellian shape of the electron energy distribution function (EEDF), as firstly observed by [4], and then confirmed by [1, 5–12]. To investigate this specific topic, an ITPA initiative is ongoing to compare data acquired from magnetic confinement machines worldwide, such as JET and W7-X (Europe), DIII-D (U.S.A.), EAST (China), and K-STAR (Korea) — see also figure 1. Dealing with different machines (in terms of geometries, heating system specifications, etc.) and diagnostics (different positions, Lines of Sight, acquisition parameters, etc.) requires a rigorously determined method of data analysis. A common approach is necessary to achieve the desired robustness in comparisons across different devices.

Based on the experience gained from recent JET data in the last experimental campaigns, in which a detailed analysis of the differences between Thomson Scattering (TS) and Electron Cyclotron Emission (ECE) was carried out, and several papers were published [1, 9–12], a set of new methods has been developed and implemented in a dedicated analysis code with the goal of supporting inter-machine comparisons. The code is designed for data management and manipulation, including various analyses, plots production, and data storage in a structured database. The data used are collected at JET by the ECE interferometer [13] and High-Resolution Thomson Scattering (HRTS) diagnostics. Detailed description of these two diagnostic systems can be found in [14, 15] and [16–18] respectively. In this paper we briefly recall their basic characteristics and Lines of Sight (LoS), as this information is essential to outline the fundamental principles behind the comparison of the two electron temperature values. In fact, the method we developed for the comparison involves both the characteristics of the measurements and the physics underlying the two diagnostics. The aim of this paper is to provide a comprehensive explanation of how the comparisons are performed and to detail the elements that ensure the reliability and robustness of the results.

The present document is structured as follows: section 2 presents the ITPA initiative and discusses the main challenges of cross-machine comparison. Section 3 addresses the fundamental issues involved in comparing electron temperature measurements obtained from different diagnostics and describes the methods implemented in the code. Finally, conclusions are drawn in section 4.

2 The ITPA activity on ‘high electron temperature measurements’

In the recent JET experimental campaigns, an international group of researchers collaborated to study the longstanding issue of the electron temperature measurements around the plasma centre, particularly when energies exceed 5–6 keV, or in conditions where ECE and Thomson Scattering measurements show values with differences well beyond the error-bars. The group builds on the previous studies mentioned above and follows up with new results [1, 9–12].

Figure 1. The tokamaks involved in the ITPA activity on ‘High electron temperature measurements’.

The comparison of the two measurements is not straightforward, as further detailed below, but the investigation into the causes behind these differences — and behind the non-Maxwellian electron distribution function — (which is beyond the scope of this paper) helps to reveal the correlations between these measurements and several critical physical aspects of the plasma under the aforementioned conditions. These include interactions between electrons and fast ions, Landau damping, Kinetic Ballooning Modes (KBMs), and the effects of the heating system [19–23].

The topic has gained growing interest in recent years, especially in view of ITER and DEMO, where the electron temperature (Te) in the plasma core is expected to exceed 20 keV, bringing renewed attention to the recent studies conducted by the ‘JET group’. A new initiative has emerged, involving various machines worldwide, within the ITPA community. The goal is to analyse the differences detected by the two diagnostics, create a database, and compare data from different machines to generalize the solution and gain a deeper understanding of the causes and the underlying physics. JET, DIII-D, EAST, K-STAR, and more recently W7-X, are currently part of this initiative, with the first experimental designs already underway at DIII-D and EAST.

Inter-machine data comparison is not trivial: each machine differs in terms of dimensions, geometries, heating systems, and diagnostic systems, including detectors (e.g., radiometers, interferometers), Lines of Sight (LoSs), toroidal and poloidal positions, as well as variations in spatial resolution, temporal resolution, integration time, and the definition of positions (via equilibrium reconstruction codes). It is essential to ensure that the comparison between the two diagnostics is performed consistently across all machines involved. To this end, building on the most recent experience gained from JET data, new methods have been defined to address most of the potential

issues arising from the differences in machine and diagnostic characteristics, and implemented in a code. The following section describes the methods in general, and how they are implemented in the code, as well as some results obtained with JET DTE3 data as examples.

3 Methods for performing the comparison

In this section, the main challenges encountered performing the comparison are described, along with an overview of the methods used to analyse the data by means of the code implemented and described step by step in section 3.1. The procedure for single-shot analysis is outlined, which can then be iterated for a series of shots to be analysed at once. The processed data are stored in a dictionary data structure (i.e., key-value pairs) and can be saved in formats such as Pickle or JSON, depending on the target platform. All procedures run automatically, facilitating multi-shot analysis, once the code is executed.

The main challenges in correctly comparing diagnostics with different characteristics lie in making the two measurements comparable from both a spatial and temporal perspective, to ensure that the comparison refers to: a) the same plasma regions for both diagnostics — the same portion of plasma, with dimensions as similar as possible — and b) to time points that are closely matched between the different signals, i.e., corresponding to the closest possible acquisition times. All other possible considerations and conclusions regarding the comparison can then be considered well-posed.

As described in more detail below, the spatial issue is addressed by averaging over the same flux coordinate intervals, ensuring similar spatial averaging for both diagnostics (and a similar number of points over which the averaging is performed). On the other hand, to align the measurements in time, the faster diagnostic is downsampled to match the temporal resolution of the slower one. Data interpolation methods were investigated to explore potential correlations with faster phenomena, however, direct comparison between the two diagnostics was performed without interpolation to avoid introducing any data manipulation. The temporal difference thus obtained between measurements is considered negligible for the scope of this study, justifying direct comparison. Where (in other machines) temporally close data is unavailable, interpolation may offer a viable alternative, as mentioned in section 3.1-STEP 5.

At this point, it is necessary to provide some details about the JET diagnostics. For further information the cited literature should be consulted [1, 11–18]. As far as this paper is concerned, the following points are of interest: Temporal and spatial resolution, and Integration over time and space of the measurements.

Temporal resolution and integration time. The ECE diagnostic (Martin-Pupplet interferometers, X-Mode, absolutely calibrated) acquires data at a rate of 60 Hz (temporal resolution of 16 ms), with an integration time of 1 ms per acquisition. Conversely, the HRTS diagnostic (incoherent Thomson scattering) has a slower acquisition rate, by a factor of three: 20 Hz, but a faster integration time equal to 10 ns. For a direct comparison, the ECE acquisition closest in time to each HRTS acquisition has been selected (as multiple ECE acquisitions occur between two HRTS acquisitions). As said, it is always possible to obtain time differences Δt on the order of the milliseconds — in any case always less than 8 ms (the maximum detected time gap) — a delay considered sufficient for this comparison ($\Delta t \ll$ acq. rate).

2025 JINST 20 C09009

Spatial resolution and volumes over which the measurements are integrated. The other fundamental aspect is the spatial resolution: from the literature, in the central plasma regions, the ECE spatial sampling is about 28 mm [14, 15], while the HRTS spatial sampling is 16 mm [17]. Vertically (in the poloidal plane), at a distance of 1 m from the antenna (i.e. the approximate magnetic axis position), considering a gaussian transverse profile with a Full Width Half Maximum (FMCW) as in (2), the ECE collect signal from an height of 36 mm (77% of the intensity within this interval) — while about 22 mm for HRTS can be considered (laser beam dimension) with a uniform profile ([16] and [17] — in particular in its figure 2-d, which shows the experimental vertical beam profile). The values here reported are obtained with a simple ray tracing, as shown in figure 2, obtained by considering a Gaussian propagation with the waist at the antenna (see eq. 1), and considering the plasma centre at 1 m from the antenna.

$$I(z,x) = I_0 \exp\left(-\frac{2z^2}{w(x)^2}\right) \tag{3.1}$$

$$\text{FWHM} = 2w(x)\sqrt{\frac{\ln 2}{2}} \tag{3.2}$$

Where I_0: max intensity, $w(x) = w_0\sqrt{1+\left(\frac{x}{x_R}\right)^2}$ is the beam dimension as a function of the distance from the waist w_0, x_R: Rayleigh length, z: transvers coordinate.

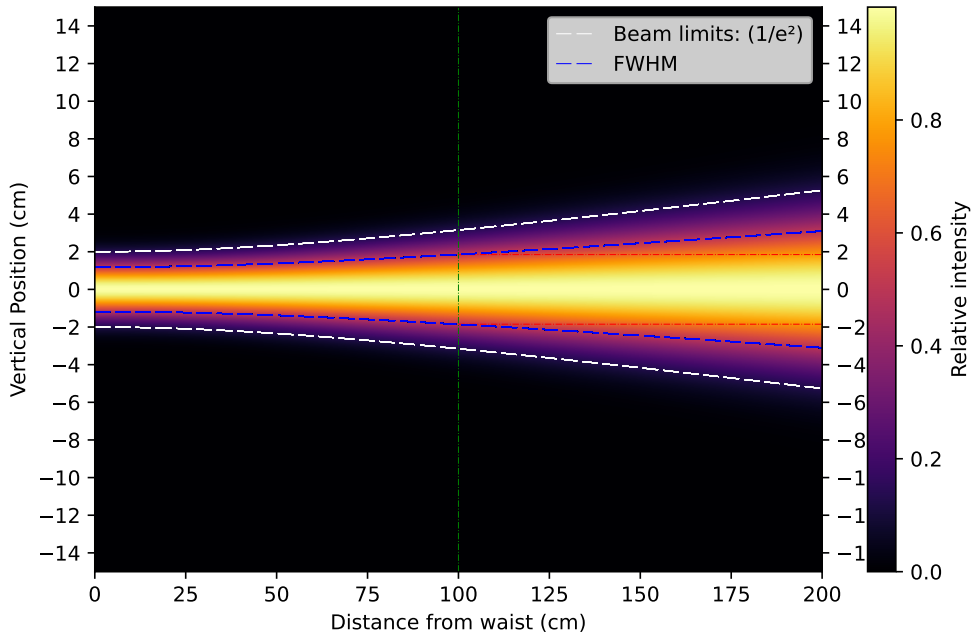

Figure 2. Ray tracing of the Gaussian propagation assumed for ECE with an antenna 4 cm in height (waist $w_0 = 2$ cm) — placed on the left-hand side of the plot. The plasma center is typically located about 1 m distance from the antenna. White curves indicate the edges, while blue curves indicate the FWHM of the gaussian profile. Thin horizontal red dashed lines project the intercept value at 77% of the intensity at 1 m distance from the antenna onto the vertical axis to aid readability. Green vertical dashed line indicates the 1 m distance from the antenna assumed as representative of the plasma center position. This is obtained by considering a toroidal magnetic field $B_t = 3,5$ T, which correspond to a second harmonic electron cyclotron emission frequency $f_{ce} = 195$ GHz, and corresponding wavelength of 1,5 mm.

2025 JINST 20 C09009

The ‘measured’ volume for each acquisition point (volume in which signal is acquired, corresponding to the scale length over which the actual profile is smoothed due to the diagnostic characteristics) can be considered as cylinders with dimensions (length along the LoS — radial x diameter of the cylinder — z-axis) approximately (28,36) mm for ECE, and (16,22) mm for HRTS.

It is worth noting that the values indicated here are estimates and may vary slightly in the plasma centre area (magnetic axis position vary with time, then the FWHM for ECE and the instrumental function for HRTS vary consequently).

For the JET-DTE3 experimental campaign, the distance between the two LoSs is approximately 5–6 cm (note that the HRTS LoS is slightly oblique, as shown in figure 3 and figure 6). To optimize the comparison, as detailed in the followings, several solutions have been adopted and an averaged measurement over an adequate length (~15 cm) around the instantaneous magnetic axis of the plasma is used for the comparison. As described in section 3.1-STEP3 this is achieved by calculating, at each acquisition time of the slowest diagnostic, the flux coordinates ρ — normalized toroidal flux (equation 3) — for the two LoSs, i.e. the equation of the LoS as a function of ρ (figure 7), and selecting instantaneous ρ intervals where both ECE and TS overlap in the same region, as close as possible to the plasma center (figure 6). In this way, the acquired data from both diagnostics are averaged at points as close to the plasma centre as possible, over a chosen length along the LoS. The averaging length can be adjusted, but the current value of 15 cm is consistent with the previous studies [1, 9, 10] and optimizes the number of measurement points included in the averaging process.

Table 1. Summary of the spatial characteristics of the two diagnostics. The data are taken from the literature [14–17]. The spatial sampling of ECE is determined by the spectral resolution of its acquisition system, and is, to a first approximation, equal to the radial resolution. The vertical resolution is evaluated as described in section 3. For HRTS, the spatial sampling is defined by the configuration of the optical fibers collecting the signal, while the radial resolution is obtained from the evaluation of the instrumental function and varies slightly with the position along the radial coordinate. The vertical resolution of HRTS corresponds more closely to the vertical extent of the scattering volume and is estimated based on the vertical laser beam size at the approximate centre of the plasma.

	Spatial sampling (mm)	Radial dimension of the scattering volume (mm)	Vertical dimension of the scattering volume (mm)
ECE	28	28	36
HRTS	17	16	22

A summary of the geometrical data related to the measurements from the two diagnostics is reported in table 1. Focusing on the poloidal plane, the following observations can be made: performing the averaging using the flux coordinate ρ implies that i) the same plasma regions are being considered, and ii) multiple measurement points along the line of sight (LoS) are included, giving robustness to the average. The overall extent of the averaging is the same for both diagnostics, ~15 cm: due to the different positions of the acquisition points, a perfectly identical extent is not achievable. Regarding the vertical extension of the integration volume, although the averaging over the ρ range accounts for it as well, it should be noted that the difference — on the order of one centimeter — can be considered negligible in plasmas with a typical radius of about one meter, as significant temperature variations are highly unlikely at this spatial scale.

2025 JINST 20 C09009

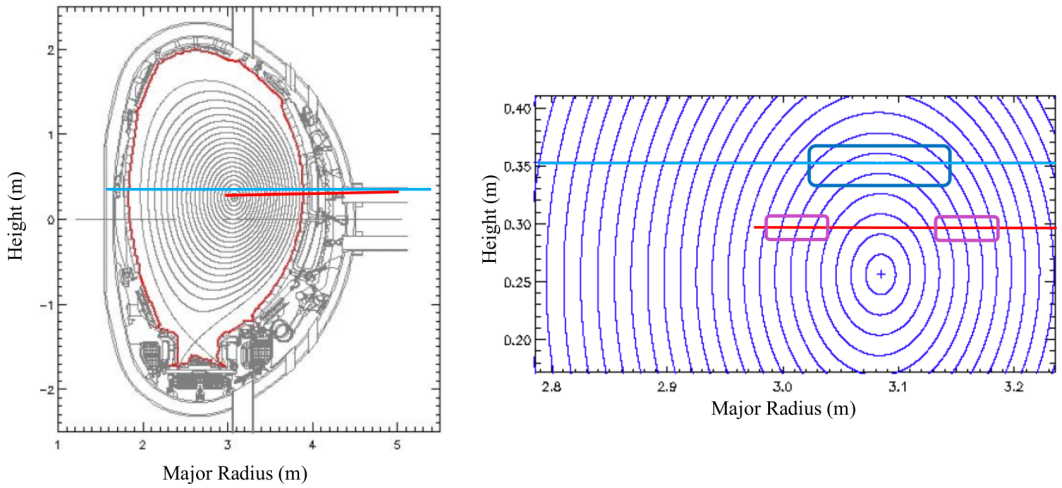

Figure 3. The equilibrium toroidal flux surfaces at a given time t are shown in grey (and blue on the right). The ECE line of sight is shown in blue, and the HRTS in red, as it is the limiter contour. The picture on the right-hand side is a zoom of the central part: as detailed in section 3.1 STEP 3, an example of the ρ range (several acquisition points) considered for the averaging is highlighted for both diagnostics at the given time t. As deeply explained in the text, an overall height of 3.6 cm is considered for ECE (blue rectangle) and 2.2 cm for HRTS (violet rectangle), over an approximate length of 13/14 cm in the direction parallel to the lines of sight for both. It is worth noting that the vertical/transverse distribution profile of the ECE-detected signal follows a Gaussian shape. The averaging volumes correspond to the same plasma regions, i.e. the same ρ coordinates.

This represents the best possible compromise for the comparison to ensure that the differences observed at high energies, are independent of the plasma position in the poloidal plane, which may be closer to one or the other LoS of the two diagnostics depending on the case (figure 6). A confirmation of the goodness is given by the fact that, in some cases and conditions, the two obtained results show agreement. These principles can be easily replicated on any machine without considering the relative positions of the lines of sight (between each other) or their position relative to the plasma. The averaging can be performed over equivalent plasma regions across different diagnostics and over similar time intervals. This ensures, in principle, the reliability of the results obtained for comparisons within a single machine while also allowing for comparability of results obtained from different machines.

3.1 The data analysis code step by step

Step 01: Time interval. The first step for each shot analysis is selecting the time interval to consider. This helps optimize the data dimension and prevents incorrect data (such as spikes or other anomalies that often occur at the temporal edges of the signal) from being included. The time window for the analysis is automatically selected by detecting when the temperature rises above a defined reference value, T_{ref} (2 keV is the value used). The initial time, t_i, and the final time, t_f, are defined as the times when the temperature crosses T_{ref} on the rising and falling edges, respectively. For this evaluation, the HRTS 'maximum temperature' data channel is used. In this step, the pulse is characterized by plotting the traces of key plasma parameters over time, such as plasma current, magnetic field, heating system power, and normalized beta — β_N —- (figure 4). Access to this plot is useful for obtaining an overview of the situation or quickly identifying any anomalies or issues once the procedure is completed. It also allows for a quick correlation of T_e differences with possible macroscopic causes.

2025 JINST 20 C09009

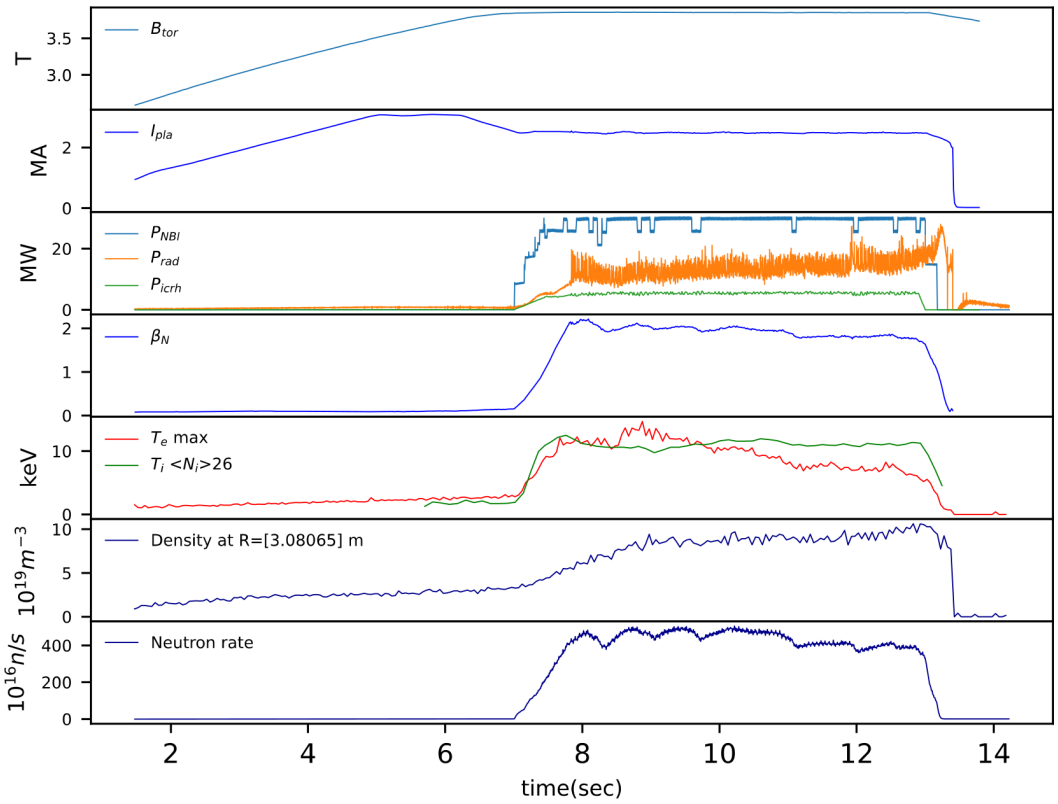

Figure 4. Traces for shot characterization. From top to bottom: toroidal magnetic field, plasma current, NBI power, ICRH power, irradiated power, normalized beta, maximum electron temperature (as measured by HRTS), ion temperature, density, and neutron rate, all plotted over time.

Additionally, a raw representation of the electron temperature time trend at a given major radius R near the plasma centre is considered (figure 5), without error bars or averaging, for the same reasons.

Step 02: Plasma position check. The second step consist in plotting the position of the plasma centre during the shot, highlighting the position within the time interval considered for the analysis — figure 6 — and giving an idea of the temporal evolution by means of a colour map. In the same plot the LoSs of the two diagnostics are shown with different colours and dashed lines. Next, the positions of the LoSs for the two diagnostics are computed with respect to the equilibrium coordinates as calculated by EFIT [24]. The position of the plasma during the shot is crucial for two main reasons: a) it allows to determine the stability of the shot being analysed, enabling immediate identification of possible anomalies; b) the position of the plasma centre relative to the LoSs could affect the measurements made with the two diagnostics, which may correspond to different points with respect to the plasma. These measurements must, therefore, be expressed in terms of equilibrium coordinates.

Step 03: Flux coordinates computation and definition of the range for the averages. As mentioned above, this is the key aspect to consider for a correct comparison. A brief note is warranted on the algorithms used for equilibrium reconstruction, which are implemented in the available codes. The positions of the data collected with ECE and TS are determined using flux surfaces and equilibrium coordinates. The calculation of these coordinates is a crucial aspect of this initiative, but it will not

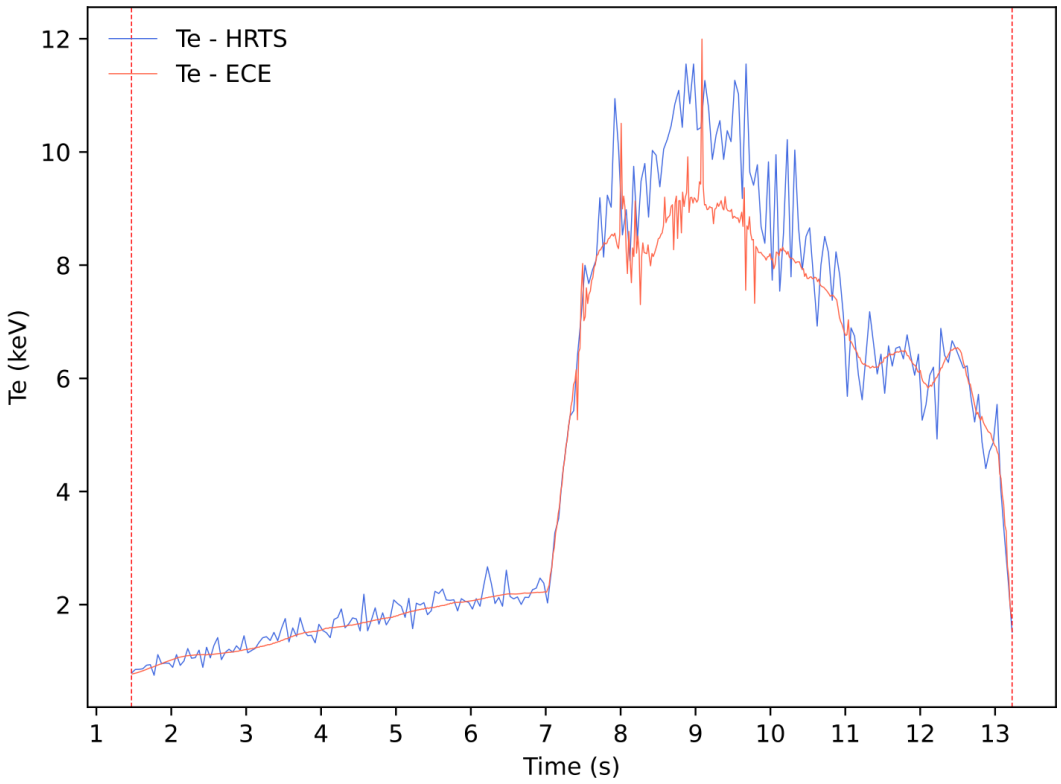

Figure 5. Electron temperature values from the ECE and TS over time at a given position in terms of major radius around the plasma center. The two red vertical dashed lines indicates the automatically selected time interval. Values from the two diagnostics are shown at their own rate without any spatial average.

be discussed in detail at this stage. Several codes are available for equilibrium reconstruction, each using data from different diagnostics for boundary conditions. For the purpose of comparing the two diagnostics and for cross-machine comparisons (where the EFIT code is always present, but other reconstruction methods are not always active on all shots), the EFIT code with magnetic constraints was chosen. This code is based on the determination of positions from the boundary conditions provided by the magnetics only. To accomplish a correct evaluation of the averaging volumes, the LoSs are computed in terms of the normalized toroidal flux coordinate at each instant. For the sake of clarity, the normalized toroidal flux (here called ρ_N) is:

$$\rho_N = \frac{\rho - \rho_{\text{axis}}}{\rho_{\text{edge}} - \rho_{\text{axis}}} \tag{3.3}$$

being $d\rho$ the toroidal flux over the infinitesimal anulus between two magnetic surfaces

$$d\rho = \oint (B_\phi dx) ds \tag{3.4}$$

Here B_ϕ is the toroidal magnetic field, dx the distance between the two magnetic surfaces, and s the surface of the anulus. Depending on the plasma position, the configuration (the equations of the LoSs as function of R and ρ) will be as in figure 7: two curves covering different regions of plasma.

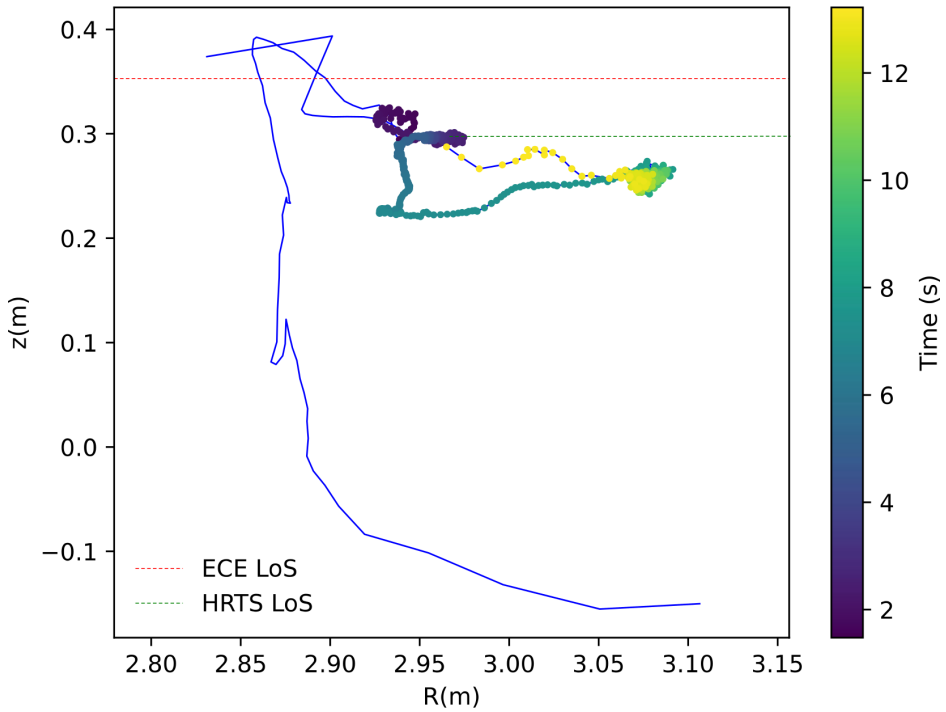

Figure 6. Plasma center (magnetic axis) position in the poloidal plane over time as resulting from the EFIT code. Red horizontal line represents the ECE Michelson line of sight, green line the HRTS LoS. In blue the magnetic axis position, highlighted with colored points when in the time interval considered for the analysis, with the color scale indicating the increasing time (right-hand side).

The range of ρ coordinates used for the averaging is computed at each acquisition time. First the greater of the two minima, $M(R_M, \rho_M)$ is selected (i.e. the closest position of the further diagnostic LoS). Half of the averaging interval $\Delta = 15$ cm is then considered, and the data point from the same diagnostics closest to $R_M \pm \Delta/2$ (point A in figure 7) determine the value ρ_{up}, which is taken as the upper limit for the estimating the ρ averaging range. To determine the lower limit ρ_{down}, the data point from the other diagnostic (the one closer to the plasma center, with the lower minimum) that is nearest (in terms of ρ) to R_M is selected (labeled B in figure 7).

This procedure defines the region closest to the magnetic axis where both diagnostics provide data, spanning approximately 15 cm in radius.

The figure 7 shows the LoSs of the two diagnostics in terms of flux coordinate vs the major radius R at a fixed time instant. In the upper plot the entire line of sight is displayed, while the lower plot provides a magnified view of the central plasma region. The circular markers indicate the measurement points (and highlighted the ones selected for the average). To consider the bigger acquisition volume of ECE, for the TS the second point below (in terms of ρ) the ECE minimum is considered (B in figure 7). In the example shown, the plasma centre at $t = 10$ s is located around $R = 3.07$ m, consistent with the position of the plasma magnetic axis observed in figure 6. Figure 7 also highlights how data are collected by the two diagnostics at different flux coordinates, and that such data are collected only within specific intervals of ρ. For instance, in the shot considered, at time t, the HRTS line of sight (shown in green) collect data only for $\rho > 0.025$, while the ECE line of sight provides measurements within $\rho > 0.060$, then acquisition point at ρ lower than 0.050

are discarded. Averaging over the central plasma region is necessary to minimize dependencies on the specific position of each diagnostic. Without such averaging, differences between diagnostic measurements would be heavily influenced by the plasma position during time.

The selection criterion defines the intervals of ρ to be considered for averaging at each instant. In figure 7, the selected values are indicated by two dashed red horizontal lines, with the corresponding averaging values highlighted in red (HRTS) and blue (ECE) for the two diagnostics. Figure 3 show a sketch of the poloidal section of JET. The magnetic equilibrium surfaces, as reconstructed by EFIT, are reported as well as the LoSs of the diagnostics in blue and red. On the right-hand side a magnification of the core with the selected ρ ranges selected (at a specific instant) are highlighted for the two LoSs.

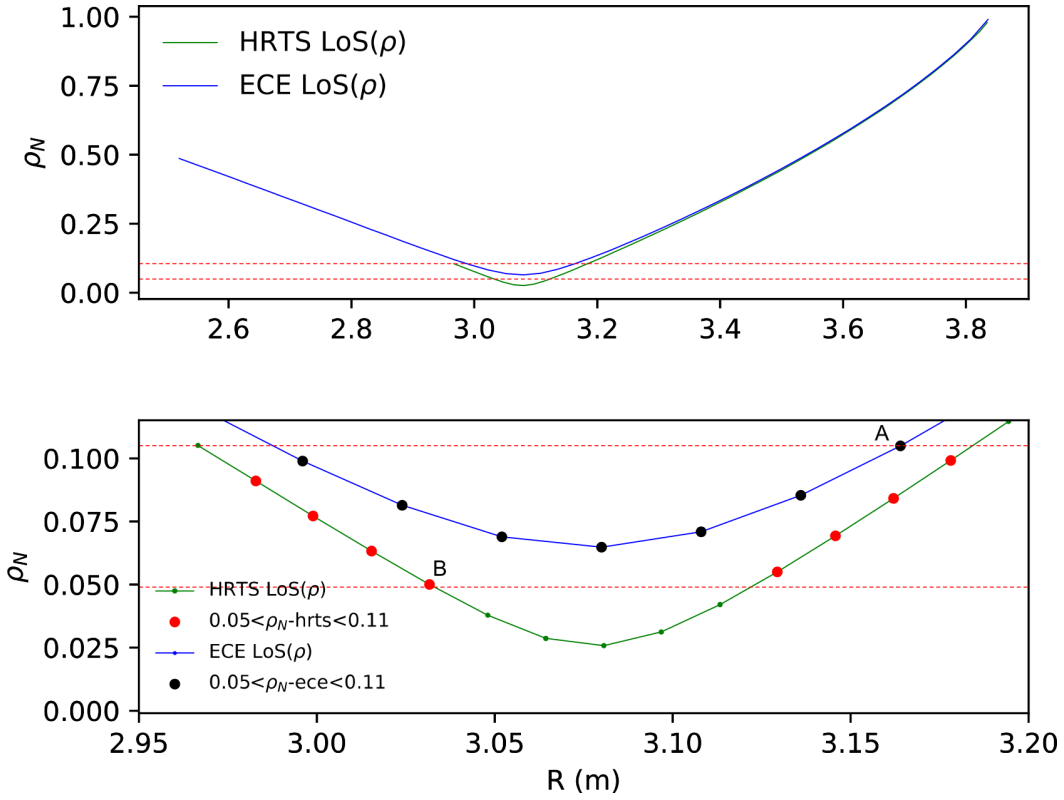

Figure 7. Diagnostic LoSs representation in terms of toroidal flux coordinate vs major radius at a fixed time instant. The upper plot shows the overall LoSs, while the lower one provides a zoomed-in view of the plasma center region. The ECE LoS is shown in blue, and the HRTS LoS in green. The horizontal red dashed lines represent the automatically selected ρ range limits for the average. The highlighted points correspond to measurement points of the diagnostics considered for the average: black for ECE and red for HRTS. The upper limit $\rho_{\text{up}} \approx 0.11$ (upper horizontal red dashed line) is determined by the point A, while the lower limit $\rho_{\text{down}} \approx 0.049$ (lower horizontal red dashed line) is given by point B.

Step 04: Common Time Axis, Averages, Errors, and Time Trends. The fourth step consists of performing a direct comparison between ECE and HRTS data. This is done by averaging values in the selected ρ range at each time instant. To ensure a common time axis, a down-sampling procedure is applied, as the ECE acquisition rate is three times higher than that of HRTS. The method simply selects the ECE time instant closest to the HRTS one, ensuring that the time gap between the two measurements is always of the order of the millisecond without requiring any data interpolation.

For averaging, an arithmetic weighted mean is used (considering a common notation, being n the number of values, x_i: the values, σ_i: error on the measurements, w_i: weights, chosen as the reciprocal of the associated errors

$$\overline{x} = \frac{\sum_1^n w_i x_i}{\sum_1^n w_i}, \quad w_i = \frac{1}{\sigma_i^2} \tag{3.5}$$

That means

$$\overline{x} = \frac{\sum_1^n \frac{x_i}{\sigma_i^2}}{\sum_1^n \frac{1}{\sigma_i^2}} \quad \text{and} \quad \sigma_{\overline{x}} = \sqrt{\frac{1}{\sum_1^n \sigma_i^{-2}}} \tag{3.6}$$

With all this considered, it is possible to directly compare the two measurements or compute their ratio, difference, etc. Figure 8 shows an example of the output, where the discrepancy between the two measurements becomes evident for T_e values above 6 keV. It is worth noting that these values result from an average, meaning they are inherently lower than the peak T_e values in the plasma centre.

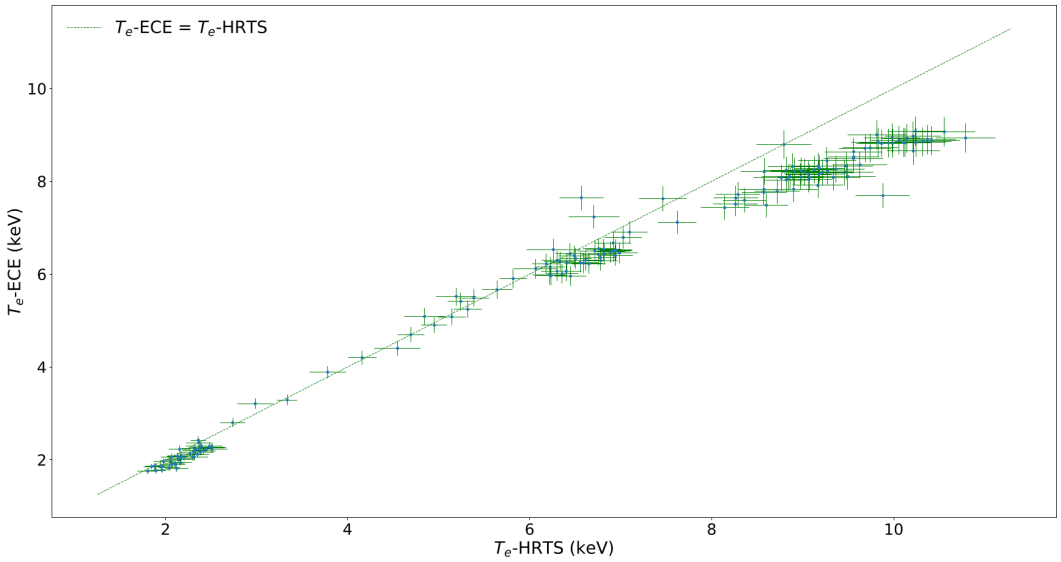

Figure 8. Direct comparison of the ECE vs HRTS measurement.

Step 05: Resampling and Interpolation for Data Comparison and Analysis. Resampling or interpolation can be applied if needed to compare data or perform additional analyses. One possible application is studying the correlation between discrepancies and MHD modes. Although not used in the current analysis, the code provides multiple options for resampling or interpolating the data, such as the 'scipy interpolate' python module, allowing for flexible and accurate processing.

Step 06: Additional Analyses and Shot Loop. With this common structure, many other analyses are possible. A couple of examples already implemented include: a) the comparison of temperature profiles at a given time, and b) the comparison of temperatures obtained from the computation of the second versus third harmonic ECE. These results may be presented in dedicated papers, as they fall outside the scope of this contribution, which focuses on the methods. Additionally, the code generates various outputs to verify the correctness of the analyses, both graphical and numerical.

4 Conclusions

Given the longstanding discrepancies in electron temperature measurements at high electron energies between ECE and Thomson Scattering diagnostics in tokamaks, and the significant efforts made over the past few decades to understand and explain these differences, new initiatives are currently underway with the aim of performing dedicated experiments, comparing data from different machines, and seeking a comprehensive explanation in view of future fusion reactors.

Comparing the two diagnostics presents challenges not only from a diagnostic perspective but also in terms of equilibrium determination, computational methodology, and, most importantly, the underlying physics responsible for the differences observed between the two measurements.

These challenges involve fundamental concepts such as temperature, energy, and thermal equilibrium. Although these topics are highly relevant to the discussion, a detailed exploration lies beyond the scope of this paper, which focuses on establishing the basis for correctly assessing the differences in the electron temperature measurements and ensuring that the results obtained from different machines are comparable. In particular, we presented a method for analysing electron temperature data obtained from the two diagnostics in the central region of the plasma (highest temperatures) and we described its implementation. This approach ensures that the results are reliable and can be meaningfully compared across the different tokamaks included in the dedicated ITPA initiative: JET, EAST, DIII-D, and W7-X.

The set of methods that has been developed is based on recent analyses performed on data from the JET DTE2 experimental campaign. The code, applied to the most recent JET DTE3 (Deuterium-Tritium) campaign data and incorporating the new HRTS line-of-sight configuration, is designed to be easily adaptable to other machines. Several key aspects are examined in detail, including the determination of the measurement point positions, the study of the measurement volumes of the two diagnostics, the identification of an instantaneous common range in equilibrium coordinates where both diagnostics are available and averages can be computed, and a brief discussion on resampling and interpolation. In particular, the open question regarding the measurement volumes and their positions has been addressed.

The detailed study of the two diagnostics and the methodological solutions presented allow us to establish that the comparison carried out under these conditions is both possible and reliable. This approach also enables the comparison of ECE and TS diagnostic results across different machines.

Indeed, without such a standardized method, variations in analysis approaches and differences in machine and diagnostic parameters would compromise the accuracy and comparability of the results. Such consistency forms the basis of the ongoing ITPA initiative on ‘High Electron Temperature Measurements’.

Acknowledgments

This work has been carried out within the framework of the ITPA joint experiment proposal - JEX #17 - on ‘High electron temperature measurements’, and under the EUROfusion Consortium has received funding from the Euratom research and training programme 2014–2018 and 2019–2020 (Grant agreement No 633053). The views and opinions express herein do not necessarily reflect those of the European Commission.

References

[1] M. Fontana et al., *High Te discrepancies between ECE and Thomson diagnostics in high-performance JET discharges*, *Phys. Plasmas* **30** (2023) 122503.

[2] D.J. Cambell et al., *ITER Research Plan*, ITR24-00005 (2024).

[3] J. Zheng et al., *Recent progress in Chinese fusion research based on superconducting tokamak configuration*, *The Innovation* **3** (2022) 100269.

[4] V. Krivenski, *Electron cyclotron emission by non-Maxwellian bulk distribution functions*, *Fusion Eng. Des.* **53** (2001) 23.

[5] E. de la Luna et al., *Impact of bulk non-Maxwellian electrons on electron temperature measurements (invited)*, *Rev. Sci. Instrum.* **74** (2003) 1414.

[6] K.V. Beausang et al., *Detecting non-Maxwellian electron velocity distributions at JET by high resolution Thomson scattering*, *Rev. Sci. Instrum.* **82** (2011) 033514.

[7] A.E. White et al., *Investigation of the Thomson scattering-ECE discrepancy in ICRF heated plasmas at Alcator C-Mod*, *Nucl. Fusion* **52** (2012) 063021.

[8] G. Giruzzi, *Electron cyclotron emission during electron cyclotron heating in tokamaks*, *Nucl. Fusion* **28** (1988) 1413.

[9] G. Giruzzi et al., *Evidence of bipolar perturbations of the electron distribution function in highperformance JET plasmas*, in the proceedings of the *29th IAEA Fusion Energy Conference*, London, United Kingdom, 16–21 October 2023.

[10] F.P. Orsitto et al., *Study on differences of ECE and high resolution thomson scattering temperature measurements in DT (deuterium-tritium) plasmas on JET*, in the proceedings of the *49th EPS Conference on Plasma Physics*, Bordeaux, France, 3–7 July 2023.

[11] M. Fontana et al., *Investigation ofTemeasurements discrepancies between ECE and Thomson diagnostics in high-performance plasmas in JET*, *EPJ Web Conf.* **277** (2023) 03006.

[12] G. Giruzzi et al., *A model of non-Maxwellian electron distribution function for the analysis of ECE data in JET discharges*, *EPJ Web Conf.* **277** (2023) 03005.

[13] A.E. Costley, R.J. Hastie, J.W.M. Paul and J. Chamberlain, *Electron Cyclotron Emission from a Tokamak Plasma: Experiment and Theory*, *Phys. Rev. Lett.* **33** (1974) 758.

[14] S. Schmuck et al., *Electron cyclotron emission spectra in X- and O-mode polarisation at JET: Martin-Puplett interferometer, absolute calibration, revised uncertainties, inboard/outboard temperature profile, and wall properties*, *Rev. Sci. Instrum.* **87** (2016) 093506.

[15] E. Luna et al., *Electron cyclotron emission radiometer upgrade on the Joint European Torus (JET) tokamak*, *Rev. Sci. Instrum.* **75** (2004) 3831.

[16] R. Pasqualotto et al., *High resolution Thomson scattering for Joint European Torus (JET)*, *Rev. Sci. Instrum.* **75** (2004) 3891.

[17] L. Frassinetti et al., *Spatial resolution of the JET Thomson scattering system*, *Rev. Sci. Instrum.* **83** (2012) 013506.

[18] M. Maslov, M.N.A. Beurskens, J. Flanagan and M. Kempenaars, *Note: Statistical errors estimation for Thomson scattering diagnostics*, *Rev. Sci. Instrum.* **83** (2012) 096106.

[19] B. Appelbe et al., *Modification of classical electron transport due to collisions between electrons and fast ions*, *Phys. Plasmas* **26** (2019) 102704.

2025 JINST 20 C09009

[20] C.H.K. Chen, K.G. Klein and G.G. Howes, *Evidence for Electron Landau Damping in Space Plasma Turbulence*, *Nat. Commun.* **10** (2019) 740 [arXiv:1902.05785].

[21] S.A. Horvath, G.G. Howes and A.J. McCubbin, *Electron Landau damping of kinetic Alfvén waves in simulated magnetosheath turbulence*, *Phys. Plasmas* **27** (2020) 102901.

[22] J. Sheffield et al., *Plasma scattering of electromagnetic radiation: theory and measurement techniques*, Academic Press (2011) [DOI:10.1016/c2009-0-20048-1].

[23] S. Mazzi et al., *Effects of Kinetic Ballooning Modes on the electron distribution function in the core of high-performance tokamak plasmas*, *Nucl. Fusion* **65** (2024) 016049.

[24] M. Brix et al., *Accuracy of EFIT equilibrium reconstruction with internal diagnostic information at JET*, *Rev. Sci. Instrum.* **79** (2008) 10F325.

2025 JINST 20 C09009